ACS APPLIED MATERIALS & INTERFACES

Research Article

Cite This: ACS Appl. Mater. Interfaces XXXX, XXX, XXX−XXX

www.acsami.org

Shear-Induced Changes of Electronic Properties in Gallium Nitride

Guosong Zeng,[†] Xiaofang Yang,[‡] Chee-Keong Tan,[§,∥] Christopher J. Marvel,[⊥] Bruce E. Koel,[‡] Nelson Tansu,[§] and Brandon A. Krick*[,†]

[†]Department of Mechanical Engineering and Mechanics, [§]Center for Photonics and Nanoelectronics, Department of Electrical and Computer Engineering, and [⊥]Department of Materials Science and Engineering, Lehigh University, Bethlehem, Pennsylvania 18015, United States

[‡]Department of Chemical and Biological Engineering, Princeton University, Princeton, New Jersey 08544, United States

[∥]Department of Electrical and Computer Engineering, Clarkson University, Potsdam, New York 13699, United States

Supporting Information

ABSTRACT: We show that sliding on the surface of GaN can permanently change the surface band structure, resulting in an increased degree of band bending by more than 0.5 eV. We hypothesize that shear and contact stresses introduce vacancies that cause a spatially variant band bending. Band bending is observed by shifts and broadening of core-level binding energies toward lower values in X-ray photoelectron spectroscopy. The extent of band bending is controlled by humidity, number of sliding cycles and applied load, presenting opportunities for scalable tuning of the degree of band bending on a GaN surface. Scanning transmission electron microscopy revealed that the epitaxy of GaN was preserved up to the surface with regions of defects near the surface. The hypothesized mechanism of band bending is shear-induced defect generation, which has been shown to affect the surface states. The ability to introduce band bending at the GaN surface is promising for applications in photovoltaics, photocatalysis, gas sensing, and photoelectrochemical processes.

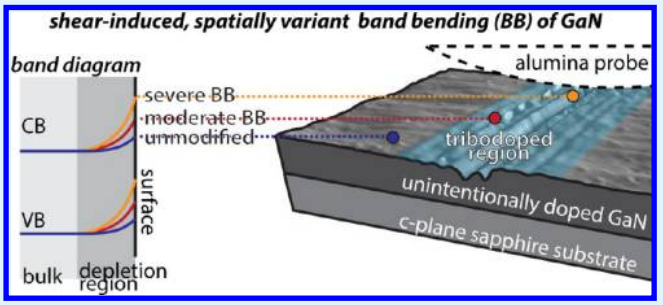

KEYWORDS: *band bending, mechanochemistry, tribochemistry, tribodoping, gallium nitride*

INTRODUCTION AND MOTIVATION

As an emerging area in controlling material properties and enhancing photoactivities for various applications, such as antibacterials, solar cells, and photocatalysts, defect engineering has attracted increasing interest from both academia and industry.[1−15] Chen et al. discovered that the surface defects in TiO_2 led to an enhancement in solar absorption activity by introducing midgap states.[1] Suntivich et al. reported that the vacancies acted as dopants and changed the spin configuration, which resulted in more efficient electron transfer.[16] Using epitaxial strain engineering to systematically tune the oxygen vacancies, Petrie et al. significantly enhanced the oxygen evolution reaction (OER) activity of a perovskite.[17] Wang et al. experimentally and computationally demonstrated the importance of oxygen vacancies in band gap narrowing of ZnO.[18] The defective ZnO obtained by ball milling showed much higher efficiency for photodecomposition of 2,4-dichlorophenol.

Mechanical work (e.g., ball milling and grinding) can introduce vacancy defects into materials, effectively doping the semiconductor; the type and quantity of defects can be controlled to obtain the desired surface properties (e.g., band structure, adsorption sites, and surface charge property). Unlike the conventional doping techniques, vacancies generated by mechanochemistry are a kind of self-doping that can preserve the intrinsic lattice structure with no foreign atoms introduced into the material and it has already been successfully used for achieving high photochemical and photocatalytic efficiencies.[18−22] Therefore, understanding the mechanisms of mechanochemical reaction-induced defect generation and the link between surface defect states and electronic properties is of paramount importance. The commonly used mechanochemical methods include ball milling, (ion-) liquid-assisted grinding, and triboadhesion;[4,14,23−28] however, each of these processes is stochastic. On the contrary, sliding experiments with single point contacts can be used to systematically study defect-induced electronic property modulation under a well-controlled contact pressure, sliding direction, speed, temperature, and environment, on either planar wafers, particles, or bulk materials. The primary limitation to sliding-induced defects is the tendency of the material to wear, but recently GaN was shown to undergo thousands of sliding cycles with remarkably low wear.[29] Combined with the knowledge that vacancies in GaN can change the band structure by introducing midgap states,[30]

Received: February 6, 2018
Accepted: June 29, 2018
Published: June 29, 2018

DOI: 10.1021/acsami.8b02271
ACS Appl. Mater. Interfaces XXXX, XXX, XXX−XXX

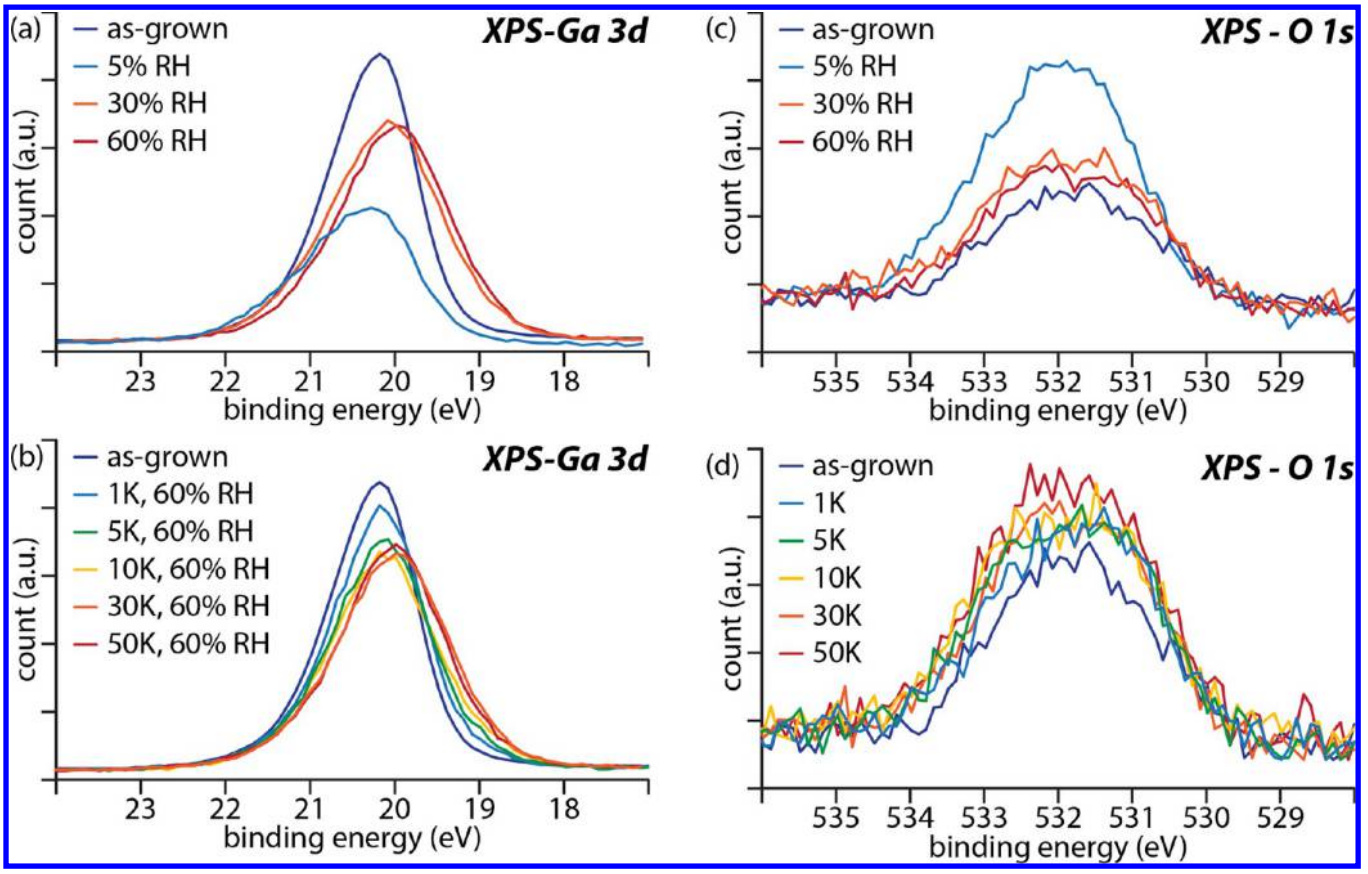

Figure 1. XPS of shear-modified GaN surfaces: (a) Ga 3d XPS spectra for different testing environments; (b) Ga 3d XPS spectra for different numbers of sliding cycles; (c) O 1s XPS spectra for different testing environments; and (d) O 1s XPS spectra for different numbers of sliding cycles.

GaN is an ideal candidate to explore shear-induced modification of electronic properties in sliding experiments.

Motivated by this, we used a ruby (single-crystal α-alumina) hemispherical probe to perform reciprocating sliding experiments on GaN under different conditions to modify the GaN surface charge property (presented as band bending here) to quantitatively link stress to electronic property modification. The enhanced surface band bending from the shear-modified surface can not only promote charge carrier transport but also suppresses electron−hole pair recombination, resulting in more efficient photoactivity.[31,32] X-ray photoelectron spectroscopy (XPS) has been extensively employed to analyze the surface chemistry and changes to the surface chemistry (tribochemistry) of the first few (1−10) nanometers of the surface in tribological contacts.[33−45] Furthermore, XPS has also been demonstrated to be a powerful tool in evaluating the surface band bending.[46−51] Thus, XPS was employed to measure the band bending and analyze the surface chemistry. Scanning transmission electron microscopy (STEM) with energy-dispersive X-ray spectroscopy (EDS) was used to visualize the shear-modified surface and subsurface. The results revealed that by adjusting the humidity, sliding cycles, and normal load, band bending of GaN can be controlled. We term this shear-induced modification to the band states as "tribodoping".

EXPERIMENTS AND METHODS

Sliding Experiments. The unintentionally doped (undoped) wurtzite single crystal (0001) 3 μm thick GaN coatings were grown by metal−organic chemical vapor deposition. Growth was performed using a low-temperature GaN nucleation layer followed by an etch-back and recovery process and high-temperature growth of GaN layers.[52] Linear reciprocating pin-on-disk sliding tests were performed by using a custom-built microtribometer[53] mounted inside a glovebox to control humidity. Three humidity levels were utilized in this study, that is, 5% RH, 30% RH, and 60% RH. All of the sliding cycle dependence and shear stress dependence studies were conducted in a 60% RH environment. All sliding tests were along the $\langle 1\bar{2}10\rangle$ crystallographic direction. Single-crystal α-alumina (ruby) balls (Swiss Jewel Company, Grade 25) with a radius of 0.75 mm were selected as the counter samples to reciprocate against the GaN coating because of their chemically inert nature, well-known hardness, and high wear resistance. The linear reciprocating sliding motion was provided by a linear motor stage (Aerotech ANT95-L) with a constant speed of 5 mm/s. The applied normal load was kept at 600 mN (±10 mN), corresponding to a maximum Hertzian contact pressure of ∼2 GPa, for all of the environment-dependence and sliding cycle-dependence studies. An additional normal load of 100 mN (∼1 GPa maximum Hertzian contact pressure) was used to investigate the role of stress magnitude.

X-ray Photoelectron Spectroscopy. The XPS analysis of the GaN samples was conducted on a ThermoFisher K-Alpha X-ray photoelectron spectrometer instrument in the Princeton Institute for the Science and Technology of Materials (PRISM) Imaging and Analysis Center at Princeton University. This system was equipped with a monochromatic X-ray source and focused lens which allows selecting an analysis area from 30 to 400 μm in 5 μm steps. The minimum spot size of 30 μm was used in this study in order to fit the XPS spot into the shear-modified surface region (wear track ∼30−80 μm wide). A conductive tape was used to ground the sample to the spectrometer, and a dual-beam (electron + ion) flood source was used to prevent sample charging during analysis. Line scans were performed through the shear-modified surfaces to include the as-

DOI: 10.1021/acsami.8b02271
ACS Appl. Mater. Interfaces XXXX, XXX, XXX−XXX

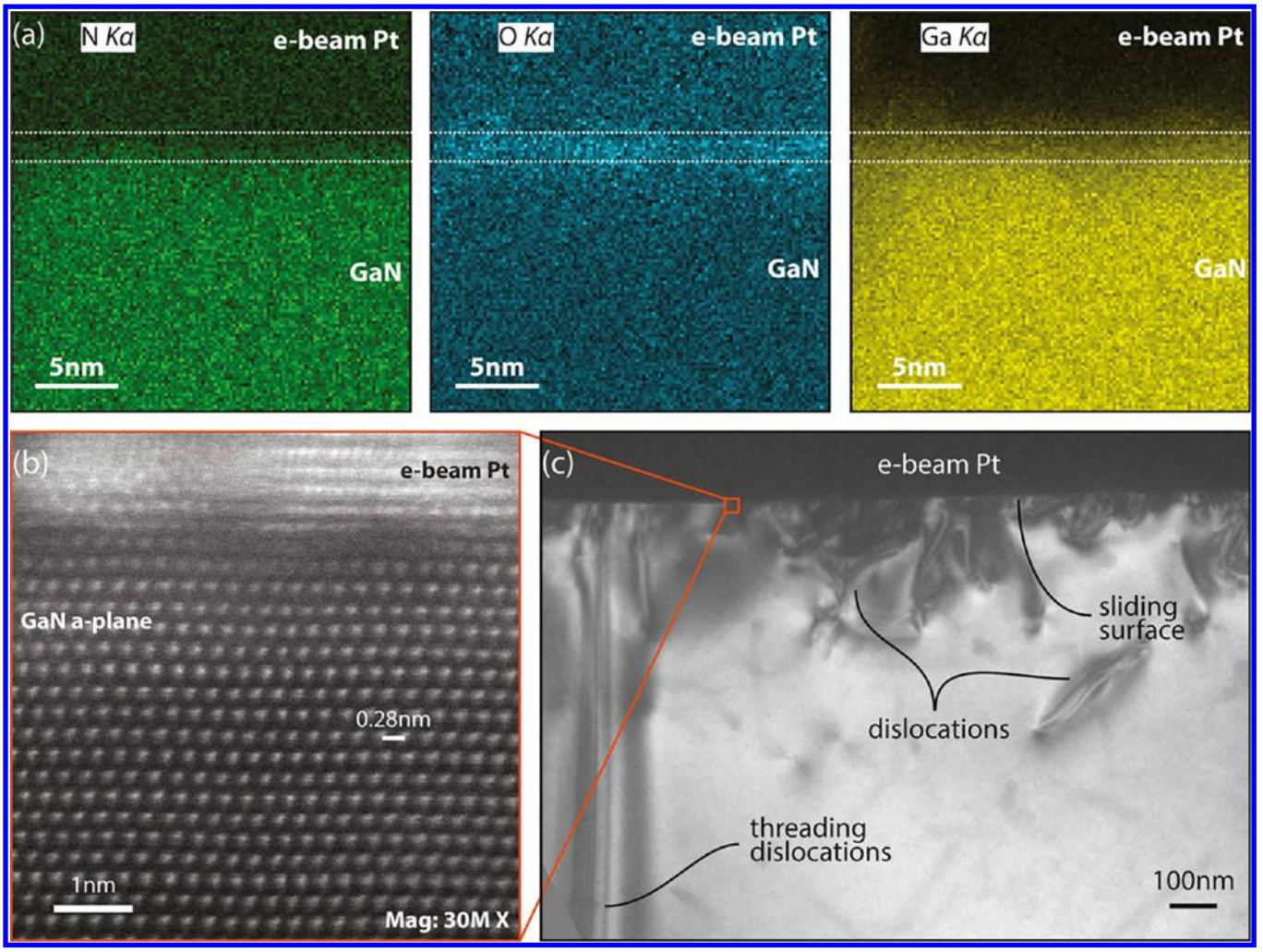

Figure 2. TEM of shear-modified surface (a) EDS showing nitrogen, oxygen, and gallium; dashed lines represent approximate location of the GaN surface. (b) High-resolution TEM image of GaN lattice after shear stress modification. (c) TEM image of sliding surface after shear stress modification.

grown surface as well as the shear-modified surface. XPS spectra of the Ga 2p, Ga 3d, N 1s, C 1s, and O 1s regions were recorded at 50 eV pass energy, and spectra with a high signal-to-noise ratio for Ga 3d, N 1s, and the Fermi edge were obtained using 100 scans. The XPS instrument was calibrated using a clean Au sample with the Fermi edge binding energy (BE) at 0.0 eV and the Au $4f_{7/2}$ peak at 84.1 eV BE.

High-Resolution TEM. The shear-modified surface obtained under 60% RH laboratory air after 30 000 sliding cycles was selected for this analysis. STEM specimens were made perpendicular to the sliding direction to expose the $(1\bar{2}10)$ plane by using a FEI Scios focused-ion beam. Protective Pt layers (250 nm thick) were deposited using electron-beam deposition, followed by ion-beam deposition of Pt (2 μm thick) to maintain the surface structure and chemistry. The specimens were sequentially thinned using 30 and 5 keV Ga ion beams, then a 900 eV Ar ion beam using a Fischione 1040 NanoMill. The subsurface atomic structure and composition were analyzed with a JEOL JEM-ARM200CF aberration-corrected STEM instrument. The STEM was operated at 200 kV and equipped with a CEOS ASCOR probe corrector and an INCA high area silicon drift detector. High-angle annular dark field (HAADF) images were acquired, and EDS maps were collected and background subtracted for the Ga Kα, N Kα, and O Kα elemental peaks.

Low-Voltage Scanning Electron Microscopy. Low-voltage scanning electron microscopy (LVSEM, ZEISS 1550) was employed to visualize the inhomogeneous band bending from the shear-modified surface (60% RH laboratory air, 30 000 sliding cycles). An in-lens detector was used to capture "true" secondary electron (SE1) signals only, and the working distance was set to be 5 mm. A low accelerating voltage (0.5 kV) was used first to obtain a clear secondary electron (SE) contrast. Then, the accelerating voltage was increased gradually to 5 kV to obtain a stable contrast reversal. This technique was previously demonstrated as a useful way to detect, map, and visualize doped regions of semiconductors by El-Gomati et al.[54,55]

Relative Peak Shift Calculations in XPS. As will be discussed and shown later in Figure 6a, the peak center (average peak shift) was obtained by calculating the center at the full width at half-maximum (fwhm), utilizing the high BE-50 (HBE-50) and low BE-50 (LBE-50) locations at 50% of the maximum peak intensity on the HBE side and LBE side, respectively. Then, the percentage of the maximum peak intensity for calculating the peak shift was changed to 15% (HBE-15 and LBE-15) for each case. The relative peak shift then was obtained by subtraction of the as-grown HBE/LBE/peak center values from the HBE/LBE/peak center values for each shear-modified surface. The location of the HBE and LBE points (intersections of the 50 or 15% lines with the spectrum) was determined by linear interpolation between data points that were closest to the 15 or 50% values of the maximum peak intensity.

RESULTS AND DISCUSSION

As shown in Figure 1a,b, sliding on the unintentionally doped (background doping is n-type, 5×10^{16} cm^{-3}) GaN surface

DOI: 10.1021/acsami.8b02271
ACS Appl. Mater. Interfaces XXXX, XXX, XXX−XXX

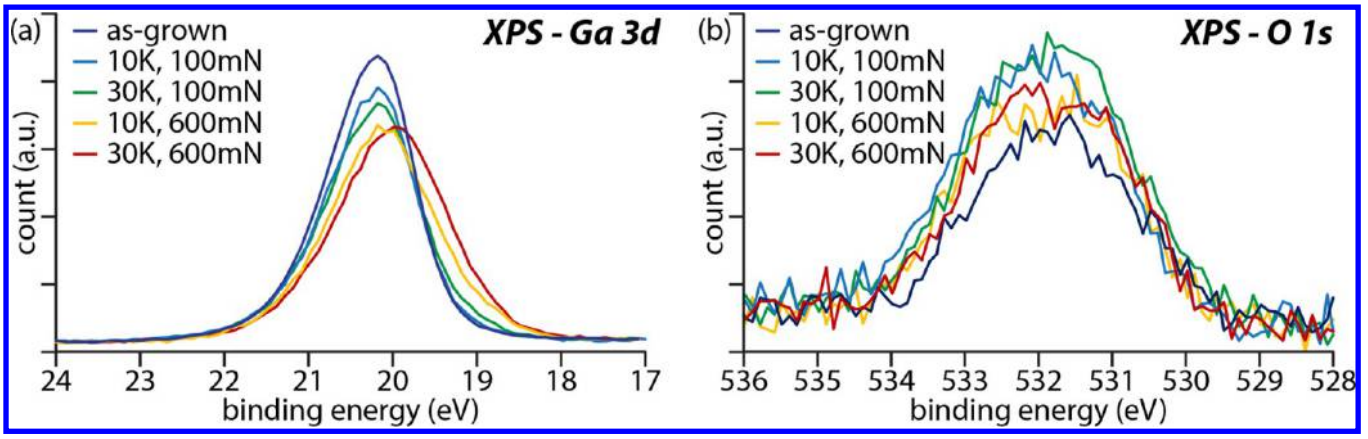

Figure 3. XPS revealing normal load and sliding cycle dependence on band bending (a) Ga 3d XPS spectra for 100 and 600 mN normal loads and (b) O 1s XPS spectra for 100 and 600 mN normal loads.

produced a significant shift to lower BE of the Ga 3d XPS peak. Calculation of the Auger parameter (see the Supporting Information: Auger parameter calculation, Table S1) and analysis of spectra obtained after deposition of Au (see below) indicate that this lower BE (rightward) shift is not chemical, i.e., it is neither caused by chemical reduction of GaN nor simply removal of the oxide layer. We hypothesize and demonstrate evidence below that this BE shift is the result of other physical changes to the GaN semiconductor surface, which results in modifying the degree of band bending. The as-grown GaN surface has a narrow Ga 3d peak at 20.2 eV, which is used as a reference peak, whereas a broader Ga 3d peak from the shear-modified surface (i.e., the region where the ruby sphere was slid against the surface) occurs at a lower BE; this is evidence that the band structure of the film has been modified. The width of this peak suggests that the band states of the shear-modified region of GaN are inhomogeneous in space. Furthermore, the Ga 2p and N 1s peaks followed similar BE shifts. However, the N 1s peak position is less reliable because there is a Ga Auger line close to the GaN N 1s BE.[56]

The degree of band structure modification (as measured by XPS) is strongly correlated with the relative humidity of the sliding environment (Figure 1a). The band structure is most modified when sliding in a 60% RH environment, followed very closely by a 30% RH environment. On contrary to that for GaN films modified in high humidity, and somewhat paradoxically, sliding in a 5% RH environment caused increased surface oxidation, as shown in Figure 1a,c.

In addition to humidity, the Ga 3d peak position also exhibited a strong dependence on the number of sliding cycles (Figure 1b). With increasing sliding cycles, the Ga 3d peak shifted further down to lower BE for up to ~30 000 sliding cycles where the maximum peak shift occurred. It is noteworthy that under the same testing environment (60% RH laboratory air), shear-modified surfaces with different sliding cycles exhibited comparable oxidation at the surface with only 50 000 cycle shear-modified surface having slightly higher O 1s signals (Figure 1d). This slightly heavier oxidation after 50 000 sliding cycles leads to a "backward" shift of the Ga 3d peak to higher BE, as shown in Figure 1b.

Several factors contribute to the peak shifts and broadening in the XPS spectra. First, sliding with a spherical probe on a flat surface results in spatially variant contact stresses applied to the film. Furthermore, wear is somewhat stochastic in nature, and the surface that is modified by sliding will be inhomogeneous. This results in a spatial variance of band bending, which indicates that the width of the broad, shifted peak is the sum of many smaller subpeaks with slightly different BEs, as shown in Figure 1a,b. As the tail shifts to lower BEs, more regions with a higher degree of band bending are observed. Second, the probe depth (surface sensitivity) of XPS is less than 8 nm, which is much smaller than the depth of the space charge layer, resulting in different BEs measured for Ga photoelectrons originating at different depths. Finally, the formation of a thin oxide at the surface can modify band bending,[57] can cause a leftward shift to higher BEs—a chemical shift competing with the band bending—and can even result in surface dipoles.[58]

The ultralow wear rate of GaN[29] allows many sliding cycles with little damage to the surface. The degree to which the surface is damaged will be important if devices are ever made using this tribodoping method. We employed TEM/EDS to visualize the crystalline structure, chemical states, and defects formed underneath the shear-modified surface. As shown in Figure 2a, the shear-modified surface was mapped by EDS and a rich oxygen signal was clearly observed. As marked by the dashed lines, the <2 nm thick oxide layer had a deficient nitrogen signal and partially deficient signal of gallium. As reported by Watkins et al.,[50] only about 0.9 monolayers of oxygen were found on the GaN surface at room temperature, which is due to the similar bond lengths for Ga−N and Ga−O that makes the GaN surface difficult to oxidize further. In our study, a larger gallium−oxygen layer was formed, likely by shear-assisted oxidation, but it is unclear if this is gallium oxide or gallium oxynitride. The shift to higher BE of the Ga peak for the 50 000 cycle sample (Figure 1b) can be attributed to increased oxidation. Longer sliding gave rise to a thicker gallium−oxygen layer. This is consistent with what we found in Figure 1b,d, that is, the XPS peak shift was not caused by band bending or chemical shift (oxidation) alone, but rather a competition between chemical (leftward) and band bending (rightward) shift.

Figure 2b shows the lattice underneath the shear-modified surface by STEM HAADF imaging. The GaN lattice maintained its wurtzite epitaxy after 30 000 sliding cycles under ~2 GPa maximum Hertzian contact pressure. From the relatively lower magnification TEM dark-field imaging (Figure 2c), it is also clear that dislocations were generated due to the shear stress. It has been experimentally and computationally demonstrated that vacancies can often be found at dislocation cores in GaN and behave as charge carriers (acceptor or

DOI: 10.1021/acsami.8b02271
ACS Appl. Mater. Interfaces XXXX, XXX, XXX−XXX

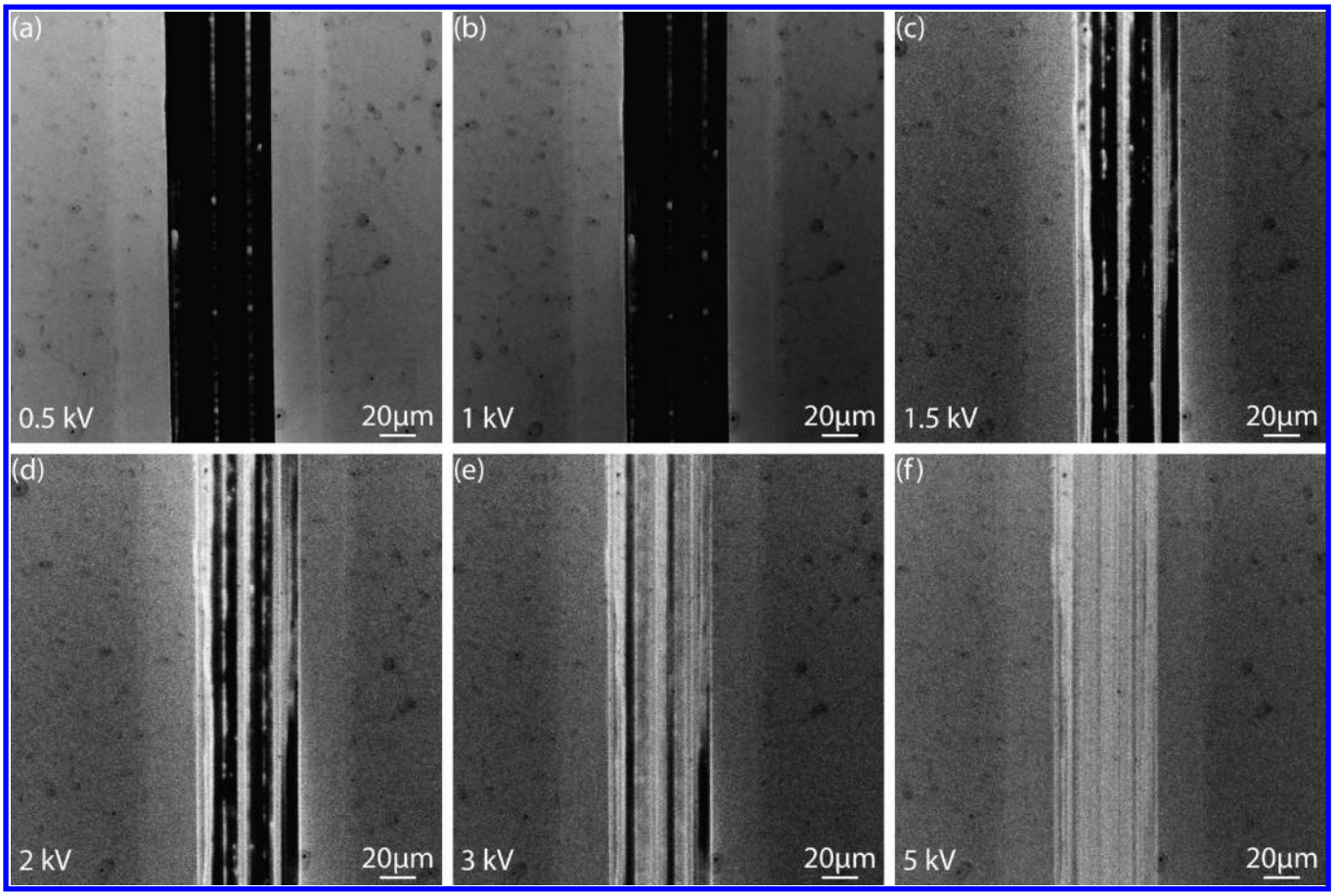

Figure 4. Visualization of the inhomogeneous shear-modified surface by LVSEM accelerating voltages were: (a) 0.5; (b) 1; (c) 1.5; (d) 2; (e) 3; and (f) 5 kV.

donor).[59−63] Thus, we hypothesize that the defects formed by shear underneath the surface introduced midgap states[30] that resulted in a surface band bending. Besides vacancy defects, an oxygen impurity incorporating with a defect site at the surface can be another possible source that gives rise to the surface band bending.[64,65] As reported elsewhere, mechanochemical methods have been extensively used to generate surface defects in semiconductor materials to enhance photocatalytic efficiency.[3−6,20,21] It has been proven that by incorporating surface defects into the material these defects can introduce midgap states and provide adsorption sites in these materials, which led to much higher photocatalytic efficiency.[1,9,12,18,66] In our discovery, the presence of defects contributes to further surface band bending, which can potentially be implemented favorably into photocatalysis and chemical-sensing devices.

To verify the role of shear stress in altering band bending, we compared the shear-modified surfaces under different normal loads of 100 and 600 mN. Figure 3a presents Ga 3d XPS spectra that probe surface band bending that results from different normal loads and different sliding cycles. Band bending still follows the sliding cycle dependence for both cases, that is, with longer sliding, the Ga 3d peak shifts further to lower BE. However, surfaces from the 100 mN normal load have significantly fewer alterations to the surface states, as evidenced by smaller intensity at lower BEs, whereas the surfaces from the 600 mN load with corresponding sliding cycles exhibited much larger peak shifts. This result is consistent with the aforementioned hypothesis that the vacancies introduced by the shear stress give rise to band bending. Figure 3b shows another interesting finding about surface oxidation, that is, counterintuitively, surfaces subjected to the higher load (600 mN) had less oxidation on the surface than those for the lower load (100 mN). We hypothesize that the frictional interaction will oxidize GaN in the presence of oxygen; however, the competition between oxide forming and oxide wearing rates results in thicker oxides for the lower applied normal loads. This can be extended to the counter-intuitive observation that lower humidity environments produced more oxide because the wear rate of GaN is significantly lower with decreasing relative humidity and this results in less wear of the oxide.

The inhomogeneity of the surface states was visualized and confirmed with LVSEM, as shown in Figure 4. The accelerating voltage of the primary electron beam was increased for Figure 4a−f and the contrast of the shear-modified region flipped as the accelerating voltage transitioned from 1 to 3 kV. The inhomogeneity observed by LVSEM can be understood as follows. Upward band bending will build up an electrical field pointing from the bulk to the surface. When applying a low accelerating voltage, this electrical field will suppress the emission of SEs from the top surface and give rise to a SE contrast (i.e., dark area in the micrograph of Figure 4a). However, with increasing accelerating voltage, the kinetic energy of the generated SEs is sufficiently large to overcome the surface electric field and eventually be detected by the detector. This is reflected in the SEM results as a partial region with larger electric field that is undetectable using certain accelerating voltages.

DOI: 10.1021/acsami.8b02271
ACS Appl. Mater. Interfaces XXXX, XXX, XXX−XXX

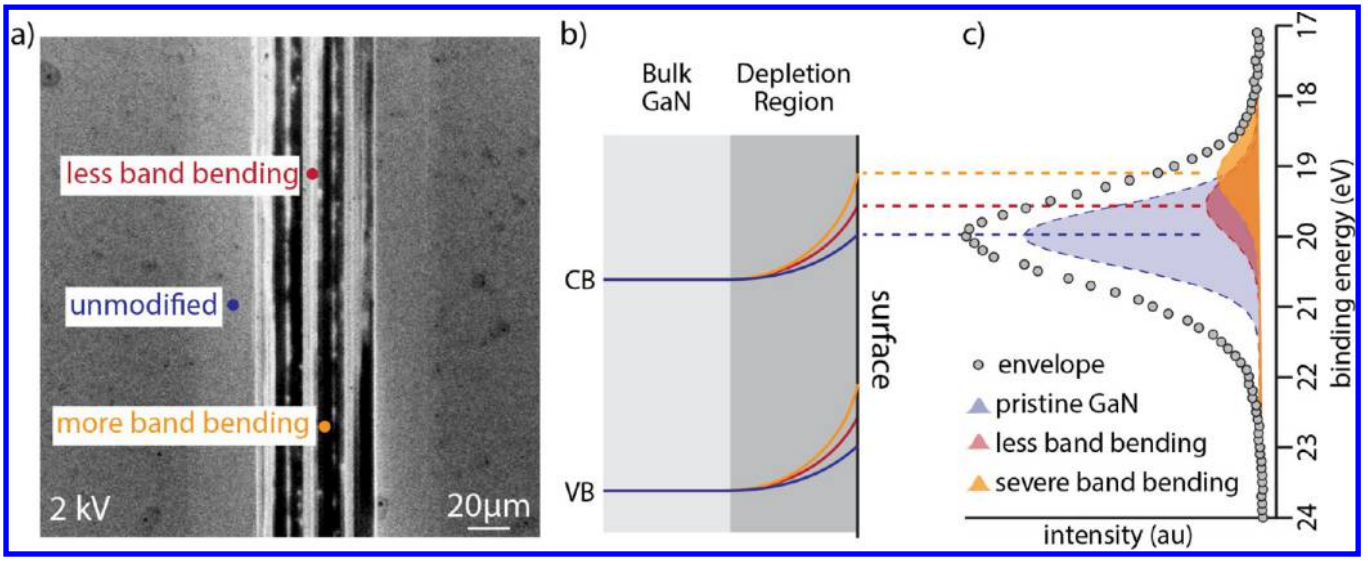

Figure 5. Schematic of inhomogeneous band bending (a) image from 2 kV LVSEM revealing spatially inhomogeneous electric field. (b) Hypothesized band diagrams for three hypothetical regions corresponding to (c) Ga 3d XPS spectrum with hypothetical peak locations caused by the band bending.

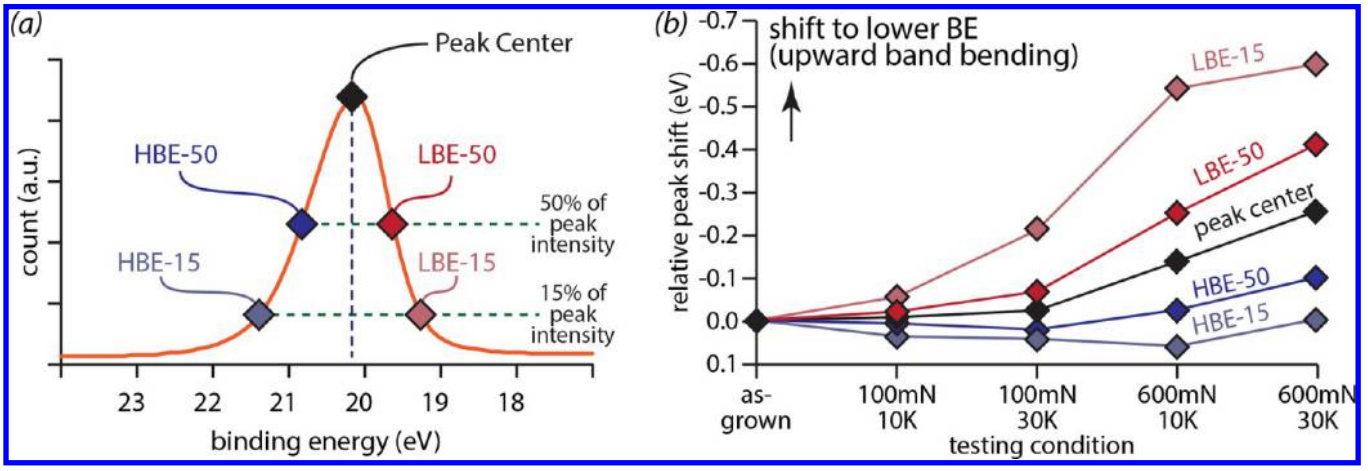

Figure 6. Summary of Ga 3d XPS peak shift and broadening. (a) Schematic identifying critical points on a Ga 3d XPS peak used in calculations probing band bending. (b) Relative shifts of these critical points due to different number of sliding cycles and applied loads. Note sign on vertical axis in (b) is inverted.

Figure 5 shows a band diagram explaining the hypothesis of inhomogeneity of band bending. When the accelerating voltage is sufficient (2 kV in this scenario) for the generated SEs to overcome the electric field in some regions that have less band bending (marked as red), those local regions can be imaged. On the other hand, the rest of the wear track with larger band bending (larger electric field) can still suppress the generation (detection) of SEs, resulting in a dark image.

As discussed earlier, the Ga 3d XPS peak shift and broadening originate from the combination of chemical shift (oxidation) and band bending (shear-induced surface charge property modification). Thus, to better understand the inhomogeneity of the surface band bending, the XPS peak shifts are revisited and the half width on both the higher and lower BE sides is examined below. The broad appearance of the Ga 3d XPS spectra for the shear-modified samples is likely due to the spectra arising from the sum of many Ga 3d peaks with centers modified by varying degrees of band bending. To quantify this, we have identified four critical points on a Ga 3d XPS peak (Figure 6a): HBE-50 and LBE-50, corresponding to the points where the intensity is equal to 50% of the maximum peak intensity on the HBE and LBE sides of the peak, respectively, and HBE-15 and LBE-15 corresponding to the points where the intensity is equal to 15% of the maximum peak intensity on the HBE and LBE sides of the peak, respectively. The value of 15% was subjectively selected to demonstrate the degree of band bending.

The relative shifts, that is, ΔHBE-50, ΔLBE-50, ΔHBE-15, and ΔLBE-15, are quantified by subtracting the as-grown values from the values obtained for the surface treatment of interest and are shown in Figure 6b. ΔLBE-50 and ΔLBE-15 increases with increasing number of sliding cycles and applied load. Both LBE-50 and LBE-15 shift toward a lower BE substantially more than the peak center. This demonstrates more locations with a higher degree of upward band bending with increasing sliding cycles and applied load. ΔLBE-15 increases substantially more with sliding cycles and applied load, to more than 0.5 eV after 10k and 30k cycles at 600 mN load; this highlights an increased percentage of the surface with band bending of at least 0.5 eV. We still must acknowledge

DOI: 10.1021/acsami.8b02271
ACS Appl. Mater. Interfaces XXXX, XXX, XXX−XXX

Table 1. Summary of Peak Critical Point Shifts

load (mN)	number of cycles	peak center shift (eV)	ΔLBE-15 (eV)	ΔLBE-50 (eV)	ΔHBE-15 (eV)	ΔHBE-50 (eV)
100	10 000	−0.007	−0.055	−0.021	0.037	0.006
	30 000	−0.023	−0.212	−0.067	0.043	0.021
600	10 000	−0.138	−0.542	−0.252	0.060	−0.025
	30 000	−0.260	−0.600	−0.413	0.004	−0.101

several alternative hypothesis that conflict with or otherwise contribute to this interpretation of the XPS shift: surface dipoles, surface oxides formed during sliding process, as well as inhomogeneous surface charging due to the morphology (differential surface charging).

There is a very small and subtle leftward shift of the HBE-50 and HBE-15 values. This shift to the higher BE (left) side relative to the as-grown peak location is attributed to oxidation. Significantly less change is observed in ΔHBE-50 and ΔHBE-15 as a function of sliding distance and applied load, revealing that oxidation is relatively small. Table 1 summarizes these shifts in all cases.

Deposition of plasmonic metals, e.g., Au, on semiconductors can form heterogeneous photocatalysts with a significant improvement in the reaction rate in various photocatalysis processes as compared to those pure semiconductor counterparts.[67−71] It has been reported that photoexcited electron−hole pairs can be effectively separated by the space charge region at the metal/semiconductor heterojunction, and this can be used to improve the efficiency of light harvesting and conversion, PEC water splitting, and so forth.[32,72] To test the potential application of the shear-induced band bending (as reported above) in photocatalysis, a <2 nm gold film was coated on the surface of both as-grown GaN and shear-modified GaN. XPS revealed that the Au 4f doublet peaks from the shear-modified surface were shifted slightly (0.11 eV) from those from the as-grown surface (Figure 7a). This peak shift is small, but significant when considering that Au is one of the most conductive metals and has been widely used in metal/GaN contacts for Fermi level alignment.[73] First, this shift indicates that even though the degree of band bending is reduced by such a thin layer of Au, the electric field originating from the shear-modified GaN surface can still affect the Au layer. This effect can lead to suppression of electron−hole pair recombination in Au films/nanoparticles and potentially result in the improvement of the efficiency of such photocatalysts. Second, this result also demonstrates that supporting Au on shear-modified GaN provides a way to tune the electronic property of Au that potentially leads to altered binding strength of adsorbates to the surface and improved catalytic properties of Au.[74] Finally, Ga 3d XPS peaks shown in Figure 7b exhibits a similar amount of shift compared to the Au 4f peaks. The Ga 3d peak of the Au-coated shear-modified GaN surface shows not only a smaller shift (0.11 eV) but also a narrower peak (by 0.5 eV) compared to the uncoated, shear-modified GaN surface shown in Figure 1a. This is in-line with our hypothesis that the broad, shifted peaks in Ga 3d spectra consist of multiple subpeaks instead of arising from a chemical shift because a thin Au layer helps to align the Fermi level, reducing the band bending variance and narrowing the peak.

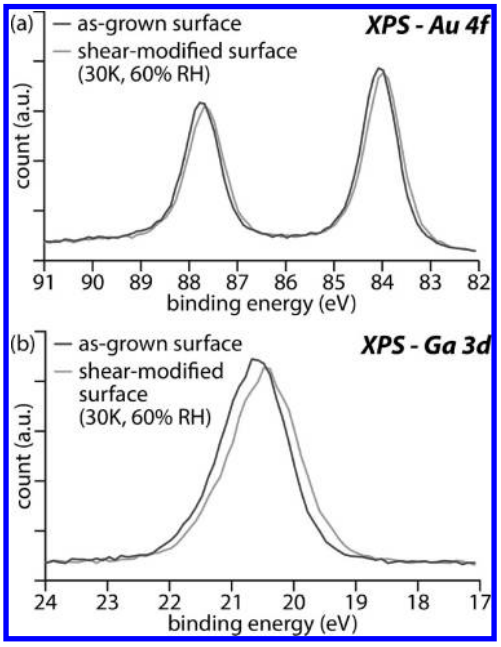

Figure 7. XPS from samples with a thin Au film deposited on top of as-deposited and shear-modified GaN surfaces: (a) Au 4f XPS spectra. (b) Ga 3d XPS spectra. Au film <2 nm to align the Fermi level.

CONCLUSIONS

We have discovered and shown that sliding on the surface of GaN can modify the band states, resulting in altered electrical properties (i.e., upward band bending of more than 0.5 eV). By using carefully controlled sliding experiments (a complementary technique to ball milling), we systematically discovered many factors that can control the degree to which band states are modified, including humidity, sliding cycles, and normal load. The shearing process modifies band bending at the GaN surface locally, which results in a large contrast of the free carriers between the sheared surface and as-grown surface. This tribodoping effect has potential for applications in a number of semiconductor devices, including those for surface-sensitive sensors (including gas sensing) and photocatalysis (including water splitting); however, its utility and scalability in industrial device fabrication must be still confirmed. This newly reported phenomenon leaves many open questions for the interdisciplinary science and engineering community, including: (1) What are the key material parameters defining the response of band bending to shear processes? (2) How can this discovery be used to develop new devices? (3) How can a larger degree of band bending be obtained to more efficiently separate electron−hole pairs for solar energy and fuels applications? and (4) Can this tribodoping method be applied to other semiconductor materials? Addressing these questions will challenge and engage interdisciplinary efforts involving chemistry, physics, materials science, tribology, and semiconductor devices.

DOI: 10.1021/acsami.8b02271
ACS Appl. Mater. Interfaces XXXX, XXX, XXX−XXX

■ ASSOCIATED CONTENT

Supporting Information

The Supporting Information is available free of charge on the ACS Publications website at DOI: 10.1021/acsami.8b02271.

Auger parameter calculation and Ga LMM Auger spectra obtained from XPS measurements (PDF)

■ AUTHOR INFORMATION

Corresponding Author

*E-mail: bakrick@lehigh.edu.

ORCID

Bruce E. Koel: 0000-0002-0032-4991

Brandon A. Krick: 0000-0003-3191-5433

Author Contributions

G.Z., B.A.K., and N.T. contributed to the initial concept development, discussions, experimental design, analysis of the results, and writing of the manuscript. X.Y. and B.E.K. contributed to XPS analysis of the samples and helped in writing of the manuscript, and C.J.M. contributed to the TEM measurements of the samples. C.-K.T. sample preparations, initial concept development, and initial discussion of the project. All the authors contributed to technical discussions of the band bending analysis for the manuscript. B.A.K. and N.T. supervised the studies performed in the manuscript.

Funding

The support of the US National Science Foundation [CMMI 1538125] (G.Z. and B.A.K.), Lehigh University Doctoral Fellowship (G.Z.), and The E. Elmer Klaus Fellowship (G.Z.) is also appreciated. The sample preparation was supported by the US National Science Foundation [ECCS 1408051 and DMR 1505122] (N.T.) and the Daniel E. '39 and Patricia M. Smith Endowed Chair Professorship Fund (N.T.).

Notes

The authors declare no competing financial interest.

All data needed to evaluate the conclusions in the paper are present in the paper and/or in the Supporting Information. Additional data related to this paper may be requested from the authors.

■ ACKNOWLEDGMENTS

The authors would like to thank Ronald A. Arif, Wei Sun, and Renbo Song (for GaN sample preparation), Nicholas C. Strandwitz, Siddha Pimputkar, Michael A. Reshchikov, Sylwia Ptasinska, and Antoine Kahn (for discussions on defect effects on band states of GaN), Henry S. Luftman (for discussions about XPS working principles and interpretation), Martin Harmer (for discussion on STEM results), Wei Sun and Damir Borovac (for their thoughtful comments and insight into band bending and surface states of GaN), Francesca M. Toma (for insights on applications and motivation) and Greg Sawyer and Rob Carpick (for general discussions on GaN tribology).

■ REFERENCES

(1) Chen, X.; Liu, L.; Yu, P. Y.; Mao, S. S. Increasing Solar Absorption for Photocatalysis with Black Hydrogenated Titanium Dioxide Nanocrystals. *Science* **2011**, *331*, 746−750.

(2) Koida, T.; Chichibu, S. F.; Uedono, A.; Tsukazaki, A.; Kawasaki, M.; Sota, T.; Segawa, Y.; Koinuma, H. Correlation between the Photoluminescence Lifetime and Defect Density in Bulk and Epitaxial ZnO. *Appl. Phys. Lett.* **2003**, *82*, 532−534.

(3) Patil, A. B.; Patil, K. R.; Pardeshi, S. K. Enhancement of Oxygen Vacancies and Solar Photocatalytic Activity of Zinc Oxide by Incorporation of Nonmetal. *J. Solid State Chem.* **2011**, *184*, 3273−3279.

(4) Beyer, M. K.; Clausen-Schaumann, H. Mechanochemistry: The Mechanical Activation of Covalent Bonds. *Chem. Rev.* **2005**, *105*, 2921−2948.

(5) Pardeshi, S. K.; Patil, A. B. Effect of Morphology and Crystallite Size on Solar Photocatalytic Activity of Zinc Oxide Synthesized by Solution Free Mechanochemical Method. *J. Mol. Catal. A: Chem.* **2009**, *308*, 32−40.

(6) Dutta, S.; Chattopadhyay, S.; Sarkar, A.; Chakrabarti, M.; Sanyal, D.; Jana, D. Role of Defects in Tailoring Structural, Electrical and Optical Properties of ZnO. *Prog. Mater. Sci.* **2009**, *54*, 89−136.

(7) Patil, A. B.; Patil, K. R.; Pardeshi, S. K. Ecofriendly Synthesis and Solar Photocatalytic Activity of S-Doped ZnO. *J. Hazard. Mater.* **2010**, *183*, 315−323.

(8) Li, Y.; Tang, Z.; Zhang, J.; Zhang, Z. Defect Engineering of Air-Treated WO_3 and Its Enhanced Visible-Light-Driven Photocatalytic and Electrochemical Performance. *J. Phys. Chem. C* **2016**, *120*, 9750−9763.

(9) Naldoni, A.; Allieta, M.; Santangelo, S.; Marelli, M.; Fabbri, F.; Cappelli, S.; Bianchi, C. L.; Psaro, R.; Dal Santo, V. Effect of Nature and Location of Defects on Bandgap Narrowing in Black TiO_2 Nanoparticles. *J. Am. Chem. Soc.* **2012**, *134*, 7600−7603.

(10) Prasanna, V. L.; Vijayaraghavan, R. Insight into the Mechanism of Antibacterial Activity of ZnO: Surface Defects Mediated Reactive Oxygen Species Even in the Dark. *Langmuir* **2015**, *31*, 9155−9162.

(11) Ling, Y.; Wang, G.; Reddy, J.; Wang, C.; Zhang, J. Z.; Li, Y. The Influence of Oxygen Content on the Thermal Activation of Hematite Nanowires. *Angew. Chem., Int. Ed.* **2012**, *51*, 4074−4079.

(12) Dong, F.; Xiao, X.; Jiang, G.; Zhang, Y.; Cui, W.; Ma, J. Surface Oxygen-Vacancy Induced Photocatalytic Activity of $La(OH)_3$ Nanorods Prepared by a Fast and Scalable Method. *Phys. Chem. Chem. Phys.* **2015**, *17*, 16058−16066.

(13) Kumar, S. G.; Koteswara Rao, K. S. R. Zinc Oxide Based Photocatalysis: Tailoring Surface-Bulk Structure and Related Interfacial Charge Carrier Dynamics for Better Environmental Applications. *RSC Adv.* **2015**, *5*, 3306−3351.

(14) James, S. L.; Adams, C. J.; Bolm, C.; Braga, D.; Collier, P.; Friščić, T.; Grepioni, F.; Harris, K. D. M.; Hyett, G.; Jones, W.; et al. Mechanochemistry: Opportunities for New and Cleaner Synthesis. *Chem. Soc. Rev.* **2012**, *41*, 413−447.

(15) Zhang, Y.; Zherebetskyy, D.; Bronstein, N. D.; Barja, S.; Lichtenstein, L.; Schuppisser, D.; Wang, L.-W.; Alivisatos, A. P.; Salmeron, M. Charge Percolation Pathways Guided by Defects in Quantum Dot Solids. *Nano Lett.* **2015**, *15*, 3249−3253.

(16) Suntivich, J.; May, K. J.; Gasteiger, H. a.; Goodenough, J. B.; Shao-horn, Y. A Perovskite Oxide Optimized for Molecular Orbital Principles. *Science* **2011**, *334*, 1383−1385.

(17) Petrie, J. R.; Jeen, H.; Barron, S. C.; Meyer, T. L.; Lee, H. N. Enhancing Perovskite Electrocatalysis through Strain Tuning of the Oxygen Deficiency. *J. Am. Chem. Soc.* **2016**, *138*, 7252−7255.

(18) Wang, J.; Wang, Z.; Huang, B.; Ma, Y.; Liu, Y.; Qin, X.; Zhang, X.; Dai, Y. Oxygen Vacancy Induced Band-Gap Narrowing and Enhanced Visible Light Photocatalytic Activity of ZnO. *ACS Appl. Mater. Interfaces* **2012**, *4*, 4024−4030.

(19) Radoi, R.; Fernández, P.; Piqueras, J.; WIggins, M. S.; Solis, J. Luminescence Properties of Mechanically Milled and Laser Irradiated ZnO. *Nanotechnology* **2003**, *14*, 794−798.

(20) Chen, D.; Wang, Z.; Ren, T.; Ding, H.; Yao, W.; Zong, R.; Zhu, Y. Influence of Defects on the Photocatalytic Activity of ZnO. *J. Phys. Chem. C* **2014**, *118*, 15300−15307.

(21) Aggelopoulos, C. A.; Dimitropoulos, M.; Govatsi, A.; Sygellou, L.; Tsakiroglou, C. D.; Yannopoulos, S. N. Influence of the Surface-to-Bulk Defects Ratio of ZnO and TiO_2 on Their UV-Mediated Photocatalytic Activity. *Appl. Catal., B* **2017**, *205*, 292−301.

DOI: 10.1021/acsami.8b02271
ACS Appl. Mater. Interfaces XXXX, XXX, XXX−XXX

(22) Zhu, Y.; Ling, Q.; Liu, Y.; Wang, H.; Zhu, Y. Photocatalytic Performance of BiPO4 Nanorods Adjusted via Defects. *Appl. Catal., B* **2016**, *187*, 204−211.
(23) Do, J.-L.; Friščić, T. Mechanochemistry: A Force of Synthesis. *ACS Cent. Sci.* **2017**, *3*, 13−19.
(24) Šepelák, V.; Düvel, A.; Wilkening, M.; Becker, K.-D.; Heitjans, P. Mechanochemical Reactions and Syntheses of Oxides. *Chem. Soc. Rev.* **2013**, *42*, 7507.
(25) Nasser, A.; Mingelgrin, U. Mechanochemistry: A Review of Surface Reactions and Environmental Applications. *Appl. Clay Sci.* **2012**, *67*−*68*, 141−150.
(26) Užarević, K.; Halasz, I.; Friščić, T. Real-Time and in Situ Monitoring of Mechanochemical Reactions: A New Playground for All Chemists. *J. Phys. Chem. Lett.* **2015**, *6*, 4129−4140.
(27) Aguilar, J. O.; Rodríguez-Lelis, J. M.; Arjona, M. J. Iron Oxide Coating Films in Soda-Lime Glass by Triboadhesion. *J. Mech. Sci. Technol.* **2009**, *23*, 1169−1174.
(28) Lelis, J. M. R.; Ocempo, J. C.; Calderón, J. P.; Robles, J. M. Deposition of Diamond in Copper by Triboadhesion. *J. Manuf. Sci. Eng.* **2003**, *125*, 628−630.
(29) Zeng, G.; Tan, C.-K.; Tansu, N.; Krick, B. A. Ultralow Wear Gallium Nitride. *Appl. Phys. Lett.* **2016**, *109*, 051602.
(30) Larson, P.; Satpathy, S. Effect of Vacancies on Ferromagnetism in GaN: Mn Dilute Magnetic Semiconductors from First-Principles. *Phys. Rev. B: Condens. Matter Mater. Phys.* **2007**, *76*, 245205.
(31) Watson, D. F.; Meyer, G. J. Electron Injection At Dye-Sensitized Semiconductor Electrodes. *Annu. Rev. Phys. Chem.* **2005**, *56*, 119−156.
(32) Zhang, Z.; Yates, J. T. Band Bending in Semiconductor Chemical and Physical Consequences at Surfaces and Interfaces. *Chem. Rev.* **2012**, *112*, 5520−5551.
(33) Bahadur, S. The Development of Transfer Layers and Their Role in Polymer Tribology. *Wear* **2000**, *245*, 92−99.
(34) Martin, J. M.; Grossiord, C.; Le Mogne, T.; Bec, S.; Tonck, A. The Two-Layer Structure of Zndtp Tribofilms: Part I: AES, XPS and XANES Analyses. *Tribol. Int.* **2001**, *34*, 523−530.
(35) Krick, B. A.; Ewin, J. J.; Blackman, G. S.; Junk, C. P.; Sawyer, W. G. Environmental Dependence of Ultra-Low Wear Behavior of Polytetrafluoroethylene (PTFE) and Alumina Composites Suggests Tribochemical Mechanisms. *Tribol. Int.* **2012**, *51*, 42−46.
(36) Pitenis, A. a.; Harris, K. L.; Junk, C. P.; Blackman, G. S.; Sawyer, W. G.; Krick, B. A. Ultralow Wear PTFE and Alumina Composites: It Is All About Tribochemistry. *Tribol. Lett.* **2015**, *57*, 4.
(37) Sawyer, W. G.; Argibay, N.; Burris, D. L.; Krick, B. A. Mechanistic Studies in Friction and Wear of Bulk Materials. *Annu. Rev. Mater. Res.* **2014**, *44*, 395−427.
(38) Aouadi, S. M.; Paudel, Y.; Luster, B.; Stadler, S.; Kohli, P.; Muratore, C.; Hager, C.; Voevodin, A. A. Adaptive Mo2N/MoS2/Ag Tribological Nanocomposite Coatings for Aerospace Applications. *Tribol. Lett.* **2008**, *29*, 95−103.
(39) Chhowalla, M.; Amaratunga, G. A. J. Thin Films of Fullerene-like MoS_2 Nanoparticles with Ultra-Low and Wear. *Nature* **2000**, *407*, 164−167.
(40) Mo, J. L.; Zhu, M. H. Sliding Tribological Behavior of AlCrN Coating. *Tribol. Int.* **2008**, *41*, 1161−1168.
(41) Kim, H.-J.; Emge, A.; Karthikeyan, S.; Rigney, D. A. Effects of Tribooxidation on Sliding Behavior of Aluminum. *Wear* **2005**, *259*, 501−505.
(42) Blanchet, T. A.; Kennedy, F. E.; Jayne, D. T. XPS Analysis of the Effect of Fillers on PTFE Transfer Film Development in Sliding Contacts. *Tribol. Trans.* **1993**, *36*, 535−544.
(43) Deli, G.; Bing, Z.; Qun-Ji, X.; Hong-Li, W. Investigation of Adhesion Wear of Filled Polytetrafluoroethylene by ESCA, AES and XRD. *Wear* **1990**, *137*, 25−39.
(44) Deli, G.; Qunji, X.; Hongli, W. ESCA Study on Tribochemical Characteristics of Filled PTFE. *Wear* **1991**, *148*, 161−169.
(45) Dudder, G. J.; Zhao, X.; Krick, B.; Sawyer, W. G.; Perry, S. S. Environmental Effects on the Tribology and Microstructure of MoS2−Sb2O3−C Films. *Tribol. Lett.* **2011**, *42*, 203−213.
(46) Caliskan, D.; Sezen, H.; Ozbay, E.; Suzer, S. Chemical Visualization of a GaN P-n Junction by XPS. *Sci. Rep.* **2015**, *5*, 10040.
(47) King, S. W.; Barnak, J. P.; Bremser, M. D.; Tracy, K. M.; Ronning, C.; Davis, R. F.; Nemanich, R. J. Cleaning of AlN and GaN Surfaces. *J. Appl. Phys.* **1998**, *84*, 5248−5260.
(48) Lorenz, P.; Gutt, R.; Haensel, T.; Himmerlich, M.; Schaefer, J. A.; Krischok, S. Interaction of GaN(0001)-2×2 Surfaces with H_2O. *Phys. Status Solidi* **2010**, *7*, 169−172.
(49) Zhang, X.; Ptasinska, S. Electronic and Chemical Structure of the H2O/GaN(0001) Interface under Ambient Conditions. *Sci. Rep.* **2016**, *6*, 24848.
(50) Watkins, N. J.; Wicks, G. W.; Gao, Y. Oxidation Study of GaN Using X-Ray Photoemission Spectroscopy. *Appl. Phys. Lett.* **1999**, *75*, 2602−2604.
(51) Bermudez, V. M. Study of Oxygen Chemisorption on the GaN(0001)-(1×1) Surface. *J. Appl. Phys.* **1996**, *80*, 1190−1200.
(52) Arif, R. A.; Ee, Y.-K.; Tansu, N. Polarization Engineering via Staggered InGaN Quantum Wells for Radiative Efficiency Enhancement of Light Emitting Diodes. *Appl. Phys. Lett.* **2007**, *91*, 091110.
(53) Erickson, G. M.; Sidebottom, M. A.; Curry, J. F.; Ian Kay, D.; Kuhn-Hendricks, S.; Norell, M. A.; Gregory Sawyer, W.; Krick, B. A. Paleo-Tribology: Development of Wear Measurement Techniques and a Three-Dimensional Model Revealing How Grinding Dentitions Self-Wear to Enable Functionality. *Surf. Topogr.: Metrol. Prop.* **2016**, *4*, 024001.
(54) El-Gomati, M.; Zaggout, F.; Jayacody, H.; Tear, S.; Wilson, K. Why Is It Possible to Detect Doped Regions of Semiconductors in Low Voltage SEM: A Review and Update. *Surf. Interface Anal.* **2005**, *37*, 901−911.
(55) El-Gomati, M. M.; Wells, T. C. R. Very-Low-Energy Electron Microscopy of Doped Semiconductors. *Appl. Phys. Lett.* **2001**, *79*, 2931−2933.
(56) Moldovan, G.; Roe, M. J.; Harrison, I.; Kappers, M.; Humphreys, C. J.; Brown, P. D. Effects of KOH Etching on the Properties of Ga-Polar n-GaN Surfaces. *Philos. Mag.* **2006**, *86*, 2315−2327.
(57) Reshchikov, M. A.; Foussekis, M.; Baski, A. A. Surface Photovoltage in Undoped N-Type GaN. *J. Appl. Phys.* **2010**, *107*, 113535.
(58) Gleason-rohrer, D. C.; Brunschwig, B. S.; Lewis, N. S. Measurement of the Band Bending and Surface Dipole at Chemically Functionalized Si(111)/Vacuum Interfaces. *J. Phys. Chem. C* **2013**, *117*, 18031−18042.
(59) Elsner, J.; Jones, R.; Heggie, M. I.; Sitch, P. K.; Haugk, M.; Frauenheim, T.; Öberg, S.; Briddon, P. R. Deep Acceptors Trapped at Threading-Edge Dislocations in GaN. *Phys. Rev. B: Condens. Matter Mater. Phys.* **1998**, *58*, 12571−12574.
(60) Weimann, N. G.; Eastman, L. F.; Doppalapudi, D.; Ng, H. M.; Moustakas, T. D. Scattering of Electrons at Threading Dislocations in GaN. *J. Appl. Phys.* **1998**, *83*, 3656.
(61) Look, D. C.; Sizelove, J. R. Dislocation Scattering in GaN. *Phys. Rev. Lett.* **1999**, *82*, 1237−1240.
(62) Wright, A. F.; Grossner, U. The Effect of Doping and Growth Stoichiometry on the Core Structure of a Threading Edge Dislocation in GaN. *Appl. Phys. Lett.* **1998**, *73*, 2751−2753.
(63) Van de Walle, C. G.; Neugebauer, J. First-Principles Calculations for Defects and Impurities: Applications to III-Nitrides. *J. Appl. Phys.* **2004**, *95*, 3851−3879.
(64) Kim, K.; Ryu, J. H.; Kim, J.; Cho, S. J.; Liu, D.; Park, J.; Lee, I.-K.; Moody, B.; Zhou, W.; Albrecht, J.; et al. Band-Bending of Ga-Polar GaN Interfaced with Al_2O_3 through Ultraviolet/Ozone Treatment. *ACS Appl. Mater. Interfaces* **2017**, *9*, 17576−17585.
(65) Patsha, A.; Sahoo, P.; Amirthapandian, S.; Prasad, A. K.; Das, A.; Tyagi, A. K.; Cotta, M. A.; Dhara, S. Localized Charge Transfer Process and Surface Band Bending in Methane Sensing by GaN Nanowires. *J. Phys. Chem. C* **2015**, *119*, 21251−21260.
(66) Kong, M.; Li, Y.; Chen, X.; Tian, T.; Fang, P.; Zheng, F.; Zhao, X. Tuning the Relative Concentration Ratio of Bulk Defects to

DOI: 10.1021/acsami.8b02271
ACS Appl. Mater. Interfaces XXXX, XXX, XXX−XXX

Surface Defects in TiO_2 Nanocrystals Leads to High Photocatalytic Efficiency. *J. Am. Chem. Soc.* **2011**, *133*, 16414−16417.
(67) Linic, S.; Christopher, P.; Ingram, D. B. Plasmonic-Metal Nanostructures for Efficient Conversion of Solar to Chemical Energy. *Nat. Mater.* **2011**, *10*, 911−921.
(68) Awazu, K.; Fujimaki, M.; Rockstuhl, C.; Tominaga, J.; Murakami, H.; Ohki, Y.; Yoshida, N.; Watanabe, T. A Plasmonic Photocatalyst Consisting of Silver Nanoparticles Embedded in Titanium Dioxide. *J. Am. Chem. Soc.* **2008**, *130*, 1676−1680.
(69) Liu, Z.; Hou, W.; Pavaskar, P.; Aykol, M.; Cronin, S. B. Plasmon Resonant Enhancement of Photocatalytic Water Splitting Under Visible Illumination. *Nano Lett.* **2011**, *11*, 1111−1116.
(70) Silva, C. G.; Juárez, R.; Marino, T.; Molinari, R.; García, H. Influence of Excitation Wavelength (UV or Visible Light) on the Photocatalytic Activity of Titania Containing Gold Nanoparticles for the Generation of Hydrogen or Oxygen from Water. *J. Am. Chem. Soc.* **2011**, *133*, 595−602.
(71) Tian, Y.; Tatsuma, T. Mechanisms and Applications of Plasmon-Induced Charge Separation at TiO_2 Films Loaded with Gold Nanoparticles. *J. Am. Chem. Soc.* **2005**, *127*, 7632−7637.
(72) Linsebigler, A. L.; Lu, G.; Yates, J. T. Photocatalysis on TiO2 Surfaces: Principles, Mechanisms, and Selected Results. *Chem. Rev.* **1995**, *95*, 735−758.
(73) Liu, Q. Z.; Lau, S. S. A Review of the Metal−GaN Contact Technology. *Solid-State Electron.* **1998**, *42*, 677−691.
(74) Yang, X.; Kattel, S.; Senanayake, S. D.; Boscoboinik, J. A.; Nie, X.; Graciani, J.; Rodriguez, J. A.; Liu, P.; Stacchiola, D. J.; Chen, J. G. Low Pressure CO2 Hydrogenation to Methanol over Gold Nanoparticles Activated on a CeO_x/TiO_2 Interface. *J. Am. Chem. Soc.* **2015**, *137*, 10104−10107.

DOI: 10.1021/acsami.8b02271
ACS Appl. Mater. Interfaces XXXX, XXX, XXX−XXX